Study of the Sea-Viewing Wide Field-of-View Sensor (SeaWiFS) aerosol optical property data over ocean in combination with the ocean color products

Menghua Wang[1]
NASA Goddard Space Flight Center, University of Maryland Baltimore County, Greenbelt, Maryland, USA

Kirk D. Knobelspiesse[2]
NASA Goddard Space Flight Center, Science Systems and Applications, Inc., Greenbelt, Maryland, USA

Charles R. McClain
NASA Goddard Space Flight Center, Greenbelt, Maryland, USA

Received 23 April 2004; revised 6 July 2004; accepted 3 August 2004; published 24 February 2005.

[1] The primary goals of the Sea-Viewing Wide Field-of-View Sensor (SeaWiFS) are to routinely provide the global ocean color and ocean bio-optical property data. In retrieving the ocean near-surface signals from SeaWiFS-measured radiances, however, the aerosol effects must be accurately estimated and removed. Therefore SeaWiFS also produces the aerosol optical property data (in particular, the aerosol optical thickness and Ångström exponent) over global ocean. Since September of 1997, SeaWiFS has generated both global aerosol (over ocean) and ocean color data for more than 6.5 years and is still in producing these products with very good sensor performance. This makes SeaWiFS the longest in history for providing simultaneously the global aerosol and ocean color products. In this paper we describe the SeaWiFS aerosol products over ocean in combination with the ocean color data. We assert through various examples that, because SeaWiFS simultaneously retrieves both atmospheric and ocean color data, the SeaWiFS products are useful to study aerosol and ocean variations in climatic forcing, biogeochemical cycling, and radiative effects in the global and regional scales.

Citation: Wang, M., K. D. Knobelspiesse, and C. R. McClain (2005), Study of the Sea-Viewing Wide Field-of-View Sensor (SeaWiFS) aerosol optical property data over ocean in combination with the ocean color products, *J. Geophys. Res.*, *110*, D10S06, doi:10.1029/2004JD004950.

1. Introduction

[2] Aerosols have been very active research areas in the recent years, in particular, satellite remote sensing of the aerosol optical and radiative properties [*King et al.*, 1999; *Kaufman et al.*, 2002]. There are various satellite sensors that have been dedicated to measure the global aerosol optical and radiative properties, e.g., the Advanced Very High Resolution Radiometer (AVHRR) [*Rao et al.*, 1989; *Husar et al.*, 1997; *Nakajima and Higurashi*, 1998; *Mishchenko et al.*, 1999; *Ignatov and Stowe*, 2002], the Moderate Resolution Imaging Spectroradiometer (MODIS) [*Kaufman et al.*, 1997; *Tanré et al.*, 1997], and the Multiangle Imaging Spectroradiometer (MISR) [*Wang and Gordon*, 1994; *Martonchik et al.*, 1998]. Satellite sensors such as the Total Ozone Mapping Spectrometer (TOMS) can provide information of the aerosol single-scattering albedo (absorbing characteristics) using the radiances measured at the UV wavelengths [*Torres et al.*, 1998], whereas the polarized radiances measured by the Polarization and Directionality of the Earth's Reflectances (POLDER) show some advantages in retrieving the aerosol optical properties over the land [*Deuze et al.*, 2001; *Tanré et al.*, 2001].

[3] Aerosols play an important role in climate radiative forcing and biogeochemical cycling [*Charlson et al.*, 1992; *Kiehl and Briegleb*, 1993]. They not only directly influence radiative transfer in the atmosphere and, hence, change the radiance reflected to space, but they also indirectly affect the radiation budget by providing cloud condensation nucleii that lead to cloud formation [*Charlson et al.*, 1987, 1992]. Aerosol particles can also deposit to and suspend within the upper layer of the ocean, thereby changing the ocean bio-optical properties and ocean productivity [*Claustre et al.*, 2002]. However, the emission of the dimethylsulfide (DMS) particles from sea surface [*Andreae et al.*, 1994; *Kettle et al.*, 1999] changes characteristics of the aerosol compositions and its radiative forcing [*Charlson et al.*, 1987].

[1]Now at NOAA National Environmental Satellite, Data, and Information Service, Office of Research and Applications, Camp Springs, Maryland, USA.
[2]Now at NASA Goddard Institute for Space Studies, New York, New York, USA.

Copyright 2005 by the American Geophysical Union.
0148-0227/05/2004JD004950

Therefore it is useful to study the aerosol global spatial and temporal variations over ocean with simultaneous ocean optical property data.

[4] The Sea-Viewing Wide Field-of-View Sensor (SeaWiFS) [*Hooker et al.*, 1992], which was launched on 1 August 1997, is primarily for the routine global ocean color measurements and ocean bio-optical property data generation. SeaWiFS has eight spectral bands centered at 412, 443, 490, 510, 555, 670, 765, and 865 nm, with bandwidth of 20 nm for the six visible bands and 40 nm for the two near-infrared (NIR) bands. For accurate ocean color measurements, SeaWiFS has very high spectral band signal-to-noise characteristics. In its more than six and half years of operation, SeaWiFS has been continuously providing high-quality ocean color products [*McClain et al.*, 2004a]. SeaWiFS ocean color products have been well established and widely used in the ocean community. For example, from a record search in the Science Citation Index (SCI) database with key word "SeaWiFS," it is found that ~450 papers have been published. These researches are mostly related to ocean property studies. In retrieving the ocean near-surface signals from SeaWiFS-measured radiances, however, the aerosol effects must be accurately estimated and removed. This is known as atmospheric correction which removes more than 90% of the sensor-observed radiance in the visible spectrum that are back-scattered from the atmosphere and ocean surface [*Gordon et al.*, 1980; *Gordon and Wang*, 1994a; *Gordon*, 1997; *Fukushima et al.*, 1998; *Antoine and Morel*, 1999]. Therefore SeaWiFS can also produce the aerosol optical property data, in particular, the aerosol optical thickness (AOT) and Ångström exponent, over global ocean [*Gordon and Wang*, 1994a; *Wang*, 2000]. The aerosol optical properties over ocean can be retrieved from other ocean color sensors such as the Medium Resolution Imaging Spectrometer (MERIS) [*Antoine and Morel*, 1999] and the Ocean Color and Temperature Scanner (OCTS) [*Fukushima et al.*, 1998]. Since September of 1997, SeaWiFS has been generating both global aerosol (over ocean) and ocean color products.

[5] In this paper, we present the SeaWiFS aerosol products over ocean in combination with the SeaWiFS ocean color products and show advantages with some examples in looking at both aerosol and ocean color data. We first briefly overview the SeaWiFS atmospheric correction and aerosol retrieval algorithms. Next, the validation descriptions and discussions that compare the SeaWiFS aerosol and ocean color data with the ground-based and in situ measurements that have been collected through the SeaWiFS and NASA Sensor Intercomparison and Merger for Biological and Interdisciplinary (SIMBIOS) [*McClain et al.*, 2002] projects are provided. Finally, we present the SeaWiFS aerosol and ocean color products over global ocean and select eight regions as examples to study their temporal and spatial variations, as well as some detailed correlation analyses between aerosols and ocean color data.

2. SeaWiFS Atmospheric Correction and Aerosol Retrieval Algorithms

[6] In this section, we briefly review the SeaWiFS atmospheric correction and aerosol retrieval algorithms, the SeaWiFS data processing procedure, as well as the SeaWiFS aerosol and ocean color products that are used in this study.

2.1. Theoretical Bases

[7] At the satellite altitude, the sensor-measured radiance at a given wavelength for the ocean-atmosphere system can be written as a linear sum from various contributions:

$$L_t(\lambda) = L_r(\lambda) + L_A(\lambda) + t(\lambda)L_{wc}(\lambda) + T(\lambda)L_g(\lambda) + t(\lambda)L_w(\lambda), \tag{1}$$

where $L_r(\lambda)$, $L_A(\lambda)$, $L_{wc}(\lambda)$, $L_g(\lambda)$, and $L_w(\lambda)$, are the radiance contributions at the top of the atmosphere (TOA) from air molecules, aerosols and Rayleigh-aerosol interactions (i.e., $L_a(\lambda)$ + $L_{ra}(\lambda)$) [*Gordon and Wang*, 1994a], whitecaps [*Gordon and Wang*, 1994b; *Frouin et al.*, 1996; *Moore et al.*, 2000], Sun glint [*Wang and Bailey*, 2001], and ocean waters, respectively. $T(\lambda)$ and $t(\lambda)$ are the atmospheric direct and diffuse transmittance [*Yang and Gordon*, 1997] at the sensor viewing direction, respectively. The water-leaving radiance $L_w(\lambda)$, which can be related to the ocean near-surface physical and bio-optical properties, is the desired quantity in the atmospheric correction for the ocean color remote sensing [*Gordon and Wang*, 1994a; *Fukushima et al.*, 1998; *Antoine and Morel*, 1999]. To remove the atmospheric effects in the derived $L_w(\lambda)$, SeaWiFS produces the normalized water-leaving radiance, $[L_w(\lambda)]_N$, which is defined as

$$[L_w(\lambda)]_N = L_w(\lambda)/\{\cos\theta_0 t_0(\lambda)\}, \tag{2}$$

where θ_0 is the solar zenith angle and $t_0(\lambda)$ is the atmospheric diffuse transmittance at the solar direction. The two-band ratio values of $[L_w(\lambda)]_N$ can then be used to derive the ocean chlorophyll-a concentration [*Gordon et al.*, 1988; *Morel*, 1988; *O'Reilly et al.*, 1998].

[8] In equation (1), the Rayleigh scattering radiance $L_r(\lambda)$ is computed using the vector radiative transfer theory (accounting for polarization) for a Rayleigh-scattering atmosphere overlying a rough (wind speed dependent) Fresnel-reflecting ocean surface [*Gordon and Wang*, 1992; *Wang*, 2002]. The whitecap radiance $L_{wc}(\lambda)$ is modeled with input of the sea surface wind speed [*Gordon and Wang*, 1994b; *Wang*, 2000]. The Sun glint $L_g(\lambda)$ is mostly avoided by titling sensor 20° away from the nadir at subsolar point and residual contamination is corrected [*Wang and Bailey*, 2001]. Thus, to derive the ocean contribution $L_w(\lambda)$ in equation (1) (ocean color products), the aerosol effects $L_A(\lambda)$ at the visible wavelengths need to be estimated. However, from aerosol contribution $L_A(\lambda)$, the aerosol optical properties can be retrieved. Therefore aerosol products are by-products from the atmospheric correction of the ocean color remote sensors [*Gordon and Wang*, 1994a].

[9] By using a set of candidate aerosol models, effects of the spectral variation of $L_A(\lambda)$ at the SeaWiFS two NIR bands centered at 765 and 865 nm can be evaluated from equation (1) because $L_w(\lambda)$ at the NIR bands are usually negligible for the open ocean waters due to strong water absorption [*Hale and Querry*, 1973; *Smith and Baker*, 1981]. For productive ocean waters (with high chlorophyll

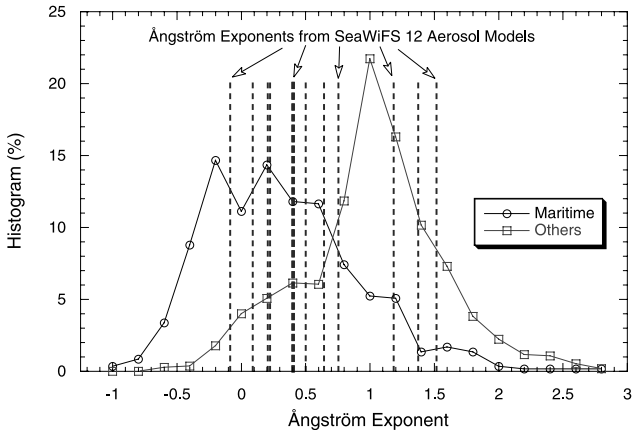

Figure 1. The Ångström exponents from the SeaWiFS 12 aerosol models compared with the results derived from the ground-based measurements. These are re-plotted from results of *Knobelspiesse et al.* [2004].

concentration), however, the NIR $L_w(\lambda)$ values are no longer negligible and can be estimated using a bio-optical model [*Siegel et al.*, 2000; *Stumpf et al.*, 2003]. Thus SeaWiFS has accounted for the ocean contributions at the NIR bands for the productive ocean waters. This is particularly important for the coastal regions where the NIR $L_w(\lambda)$ values are usually significant [*Siegel et al.*, 2000; *Stumpf et al.*, 2003]. The $L_A(\lambda)$ values that are derived in the SeaWiFS NIR bands, i.e.,

$$L_A(\lambda) = L_t(\lambda) - L_r(\lambda) - tL_{wc}(\lambda) - TL_g(\lambda) - tL_w(\lambda), \qquad (3)$$

are then used to select two most appropriate aerosol models from a suite candidate aerosol models. A weight that is best fit to the measured NIR radiances from the radiances computed using the two selected aerosol models is estimated. Using the two aerosol models with a weight and the SeaWiFS-measured radiance, the AOT at 865 nm $\tau_a(865)$ (or $\tau_a(\lambda)$ for all the SeaWiFS wavelengths) and Ångström exponent from wavelengths 510 and 865 nm $\alpha(510)$ can then be retrieved [*Gordon and Wang*, 1994a; *Wang*, 2000]. The Ångström exponent $\alpha(\lambda)$ is defined as

$$\alpha(\lambda) = \log_e\left(\frac{\tau_a(\lambda)}{\tau_a(865)}\right) / \log_e\left(\frac{865}{\lambda}\right), \qquad (4)$$

where $\tau_a(\lambda)$ is the AOT at the wavelength λ. Therefore SeaWiFS algorithm uses aerosol spectral information from two-band measurements to derive appropriate aerosol models and aerosol optical properties [*Gordon and Wang*, 1994a]. Two-band approach in deriving aerosol optical properties is also discussed by other investigators [e.g., *Nakajima and Higurashi*, 1998; *Mishchenko et al.*, 1999].

[10] For the atmospheric correction, the $L_A(\lambda)$ radiances derived in the SeaWiFS NIR bands are extrapolated into the visible wavelengths. This can be achieved using the derived aerosol models and the AOT $\tau_a(865)$ through the radiative transfer computations. The normalized water-leaving radiances $[L_w(\lambda)]_N$ at the visible wavelengths are then retrieved through equations (1) and (2), and the chlorophyll-a concentration Chl-a is obtained using the two-band ratio value of the derived $[L_w(\lambda)]_N$ [*O'Reilly et al.*, 1998]. This is a typical two-step atmospheric correction procedure in which the atmosphere and ocean are assumed to be de-coupled [*Gordon and Wang*, 1994a; *Gordon*, 1997; *Fukushima et al.*, 1998; *Antoine and Morel*, 1999].

2.2. Aerosol Models for the SeaWiFS Lookup Tables

[11] A set of realistic aerosol models is needed for the atmospheric correction and aerosol retrievals. The current SeaWiFS algorithm uses 12 aerosol models for generating the aerosol lookup tables [*Wang*, 2000]. They are the oceanic model with the relative humidity (RH) of 99% (denoted as O99), the maritime model with RH of 50%, 70%, 90%, and 99% (denoted as M50, M70, M90, and M99), the coastal model with RH of 50%, 70%, 90%, and 99% (denoted as C50, C70, C90, and C99), and the tropospheric model with RH of 50%, 90%, and 99% (denoted as T50, T90, and T99). The oceanic, maritime, and tropospheric models are from *Shettle and Fenn* [1979] and also provided in the work of *d'Almeida et al.* [1991], whereas the coastal model was introduced in the work of *Gordon and Wang* [1994a]. In these 12 aerosol models, the single-scattering albedo at 865 nm varies from 0.930 for the T50 model to 1.0 for the O99 model, while the Ångström exponent $\alpha(510)$ changes from -0.087 for the O99 model to 1.53 for the T50 model. Figure 1 is a re-plot of results from *Knobelspiesse et al.* [2004] comparing the Ångström exponents from the SeaWiFS 12 aerosol models with those of the ground-based measurements. The Ångström exponent values for the SeaWiFS 12 aerosol models are represented as vertical dashed lines that are compared with the histograms from the ground-based data collected by the SIMBIOS project (see discussions also in section 3). Clearly, the in situ Ångström exponents obtained from maritime environment can be well represented with the SeaWiFS 12 aerosol models most of the time. For aerosols with very large Ångström exponents, e.g., >1.5, the current SeaWiFS models may not be representative. Therefore the SeaWiFS aerosol models represent mostly the nonabsorbing and weakly absorbing aerosols that are usually present in the ocean maritime environment.

2.3. SeaWiFS Data Processing and Products

[12] Since September of 1997, SeaWiFS routinely provides ocean color and atmospheric products, e.g., the normalized water-leaving radiance $[L_w(\lambda)]_N$ for six visible wavelengths (412, 443, 490, 510, 555, and 670 nm), chlorophyll-a concentration Chl-a, AOT at 865 nm $\tau_a(865)$, and the aerosol Ångström exponent derived from the wavelength 510 and 865 nm $\alpha(510)$. SeaWiFS has gone through four major reprocessings of the entire data set. Each reprocessing has addressed the data quality issues that are related to the sensor calibration, instrument navigation, data masks and flags, and retrieval algorithms. The SeaWiFS data used in here are from the fourth data reprocessing which was carried out in July 2002 [*Patt et al.*, 2003]. Currently, the SeaWiFS data processing is optimized for the ocean color measurements (e.g., chlo-

rophyll-a concentration). Very high AOT data such as the dust and smoke plumes are usually masked out due to large uncertainties in the ocean color products with these cases [*Gordon*, 1997]. The SeaWiFS has a reflectance threshold at 865 nm corresponding to the AOT of ~0.3. Thus the current SeaWiFS aerosol products are mostly applicable and valid in the open ocean regions where the marine aerosols are often the dominant sources.

[13] It is noted that, however, the SeaWiFS measurements can be used to derive the aerosol optical properties for very thick aerosol layers, e.g., for the dust study [*Husar et al.*, 2001; *Moulin et al.*, 2001a], and possibly for the ocean color data in the regional case study [*Moulin et al.*, 2001b]. Implementation is planned for an aerosol retrieval scheme in which very high AOT (e.g., dust and smoke) can still be retrieved even though the ocean color data may have large uncertainties. In these cases, flags can be applied to the ocean color products.

3. SeaWiFS Data Compared With the Ground-Based Measurements

[14] In this section, we provide some validation results in which the SeaWiFS aerosol and ocean color products are compared with the in situ and ground-based measurements. The in situ and ground-based data were obtained through the calibration and validation efforts under the SeaWiFS and the SIMBIOS projects. Brief discussions are also provided for comparisons of the SeaWiFS AOT product with data derived from the other satellite sensors.

3.1. Data From Ground-Based Measurements

[15] Since 1997, the SeaWiFS and the SIMBIOS projects have funded the collection of high quality ocean in situ data and atmosphere ground-based measurements as a prerequisite for satellite data product validation, algorithm development, satellite data comparison and intercalibration [*Wang and Franz*, 2000; *Wang et al.*, 2002], and data merger studies and time series analyses [*Gregg et al.*, 2002; *Maritorena et al.*, 2002]. The SeaWiFS Bio-optical Archive and Storage System (SeaBASS) [*Werdell et al.*, 2003] maintains a local repository of in situ ocean bio-optical data to support and sustain regular scientific analyses. Within the SIMBIOS project, a pool of Sun photometers and above-water radiometers has been maintained and deployed in the various field campaigns to complement in-water optical measurements and the Aerosol Robotics Network (AERONET) [*Holben et al.*, 1998]. The SIMBIOS project has also contributed 12 CIMEL automated Sun/sky photometers for the AERONET in which they are deployed at coastal and island locations. Currently, SeaBASS has archived data from over 1150 field campaigns, collected by ~60 contributors at over 44 institutions in 14 countries [*Fargion and McClain*, 2003]. The SIMBIOS project office has used a rigorous series of data submission protocols and quality control metrics to maintain consistent and high quality data [*Mueller and Fargion*, 2002; *Knobelspiesse et al.*, 2004]. The aerosol optical property data are mostly collected using the instrument pool of 14 Microtops II Sun photometers [*Morys et al.*, 2001], one SIMBAD and two SIMBADA above-water radiometers/Sun photometers [*Deschamps et al.*, 2004], and one micropulse lidar. There are also significant aerosol data acquired with the ship-mounted marine shadow-band radiometers [*Reynolds et al.*, 2002]. Detailed description of the SIMBIOS aerosol optical property data that are archived in the SeaBASS is provided in the work of *Knobelspiesse et al.* [2004].

3.2. Comparisons Between SeaWiFS and Ground-Based Measurements

[16] We compare the SeaWiFS atmospheric and ocean color products with data from the in situ and ground-based measurements. We select the nonrestrict (after three years of data restriction) in situ and ground-based data from the SeaBASS database in this study. All in situ and ground-based data presented in here were acquired nearly simultaneously with the SeaWiFS measurements (within ±3 hours). The red and green dots in Figure 2 show the geolocations of the ground-based and in situ measurements acquired for aerosol (red) and ocean color (green) product comparisons in this study. Figure 3 provides results for the SeaWiFS aerosol and ocean color products compared with the in situ and ground-based measurements. Figures 3a and 3b show comparison results for $\tau_a(\lambda)$ at 865 nm and at the various visible wavelengths, while Figures 3c and 3d are results for $[L_w(\lambda)]_N$ at the visible wavelengths and chlorophyll-a concentration. In general, good agreements are achieved for the SeaWiFS atmospheric and ocean color products in comparing with the ground-based and in situ data. For the atmospheric products, Figure 3a shows a slight over-estimation of the SeaWiFS $\tau_a(865)$ in comparing with the ground-based measurements. These are indicated by a linear fit for data sets with slope of 0.9810, intercept of 0.0211, and correlation coefficient of 0.8394. However, the entire spectral $\tau_a(\lambda)$ data comparisons (Figure 3b) show relative flatter spectral $\tau_a(\lambda)$ (with respect to wavelength) from SeaWiFS than those from the ground-based measurements. The slope of linear fit for $\tau_a(\lambda)$ comparison decreases with decrease of the wavelength, indicating under-estimation of the aerosol Ångström exponent. We use the spectral $\tau_a(\lambda)$ data instead of $\alpha(510)$ for comparison because Ångström exponent depends on the wavelength. The ocean color product comparisons show quite good agreements between SeaWiFS and in situ data. Figures 3c and 3d show that slope of 0.9852, intercept of 0.0559, and correlation coefficient of 0.9447 are obtained for the $[L_w(\lambda)]_N$ data, while these values are 0.9552 (slope), −0.0624 (intercept), and 0.9332 (correlation coefficient) in log scale for the chlorophyll-a concentration comparisons. It is noted that the comparison results presented in here for both aerosol and ocean color products include cases with both case 1 (open oceans) and case 2 (most in coastal regions) waters. Some detailed validation analyses for the SeaWiFS ocean color products are discussed in the work of *McClain et al.* [2004a].

3.3. Comparisons With Other Data Sets

[17] The detailed comparisons and analyses of the satellite-derived AOT over ocean from total of nine aerosol retrieval algorithms, which includes algorithms for data

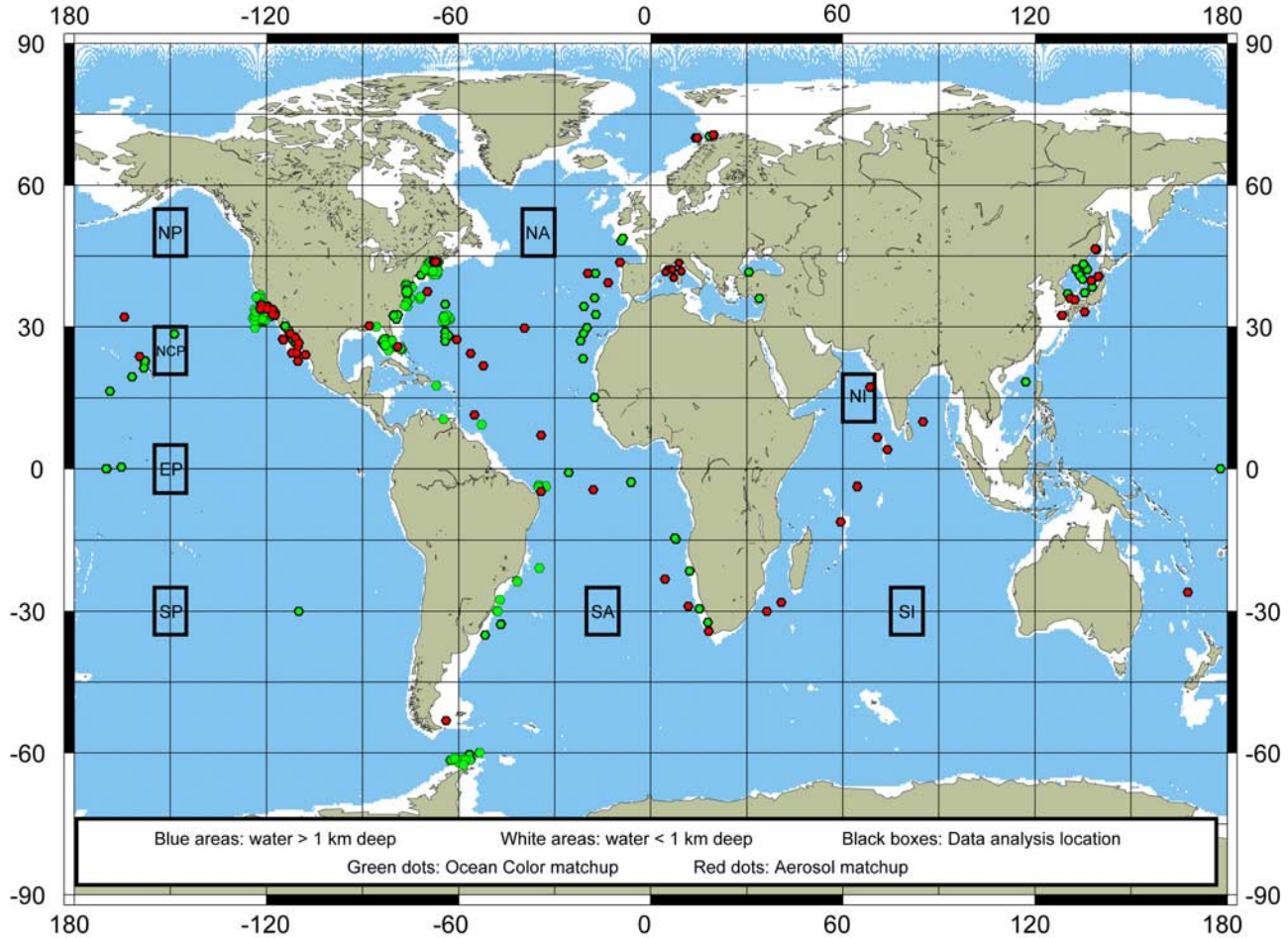

Figure 2. Global images indicating the global water deeper than 1 km (blue areas), the ground-based measurements for aerosol (red dots), the in situ data for the ocean color (green dots), and the selected eight regions for the SeaWiFS data analyses (black boxes).

measured by AVHRR, TOMS, SeaWiFS, MODIS, MISR, and some other sensors, have been carried out by *Myhre et al.* [2005]. In that study, the satellite results are also compared with the ground-based data from AERONET [*Holben et al.*, 1998]. Although some good agreements are found within various satellite data products, significant differences in the derived AOT from various satellite sensors, in particular, at the high latitude regions (e.g., southern oceans), are reported [*Myhre et al.*, 2005]. This is true even for sensors dedicated for the aerosol measurements. In general, for cases with not too large AOT, the SeaWiFS AOT is compared well with the AERONET ground-based measurements and with results derived from some of sensors (e.g., AVHRR, MODIS) [*Myhre et al.*, 2005]. SeaWiFS aerosol product shows high stability and usually has the lowest data variation (standard deviation) in all the data sets. However, for cases with the high AOT (e.g., dust and smoke plumes), the SeaWiFS aerosol product shows large differences comparing with other data sets because SeaWiFS has a reflectance threshold at 865 nm to optimize data processing for the ocean color products. There are various factors that may contribute the significant differences in the derived AOT within various satellite sensors, e.g., the sensor calibration, algorithm performance, radiative transfer modeling (lookup tables), cloud masking, Sun glinting masking and correction, and data sampling issues (both temporal and spatial). Clearly, further study to understand these differences is needed.

4. Regional Time Series of the SeaWiFS Atmospheric and Ocean Products

[18] Because SeaWiFS simultaneously retrieves both atmospheric and ocean color products, we can study the aerosol and ocean color products collectively. In this section, the SeaWiFS aerosol and ocean color products from global deep water are presented. We then select eight regions in the global oceans to provide examples of the temporal and spatial variations of the aerosol and ocean color optical properties from the SeaWiFS measurements.

4.1. Products Stability and Repeatability in the Global Deep Water

[19] Figure 4 provides the mean values of the SeaWiFS-derived products as a function of time (SeaWiFS entire mission from September 1997 to March 2004) for AOT $\tau_a(865)$, Ångström exponent $\alpha(510)$, the normalized water-leaving radiance at 443 nm $[L_w(443)]_N$, and the chlorophyll-a concentration Chl-a. These data were derived from the SeaWiFS 8-day global deep water regions (deeper than

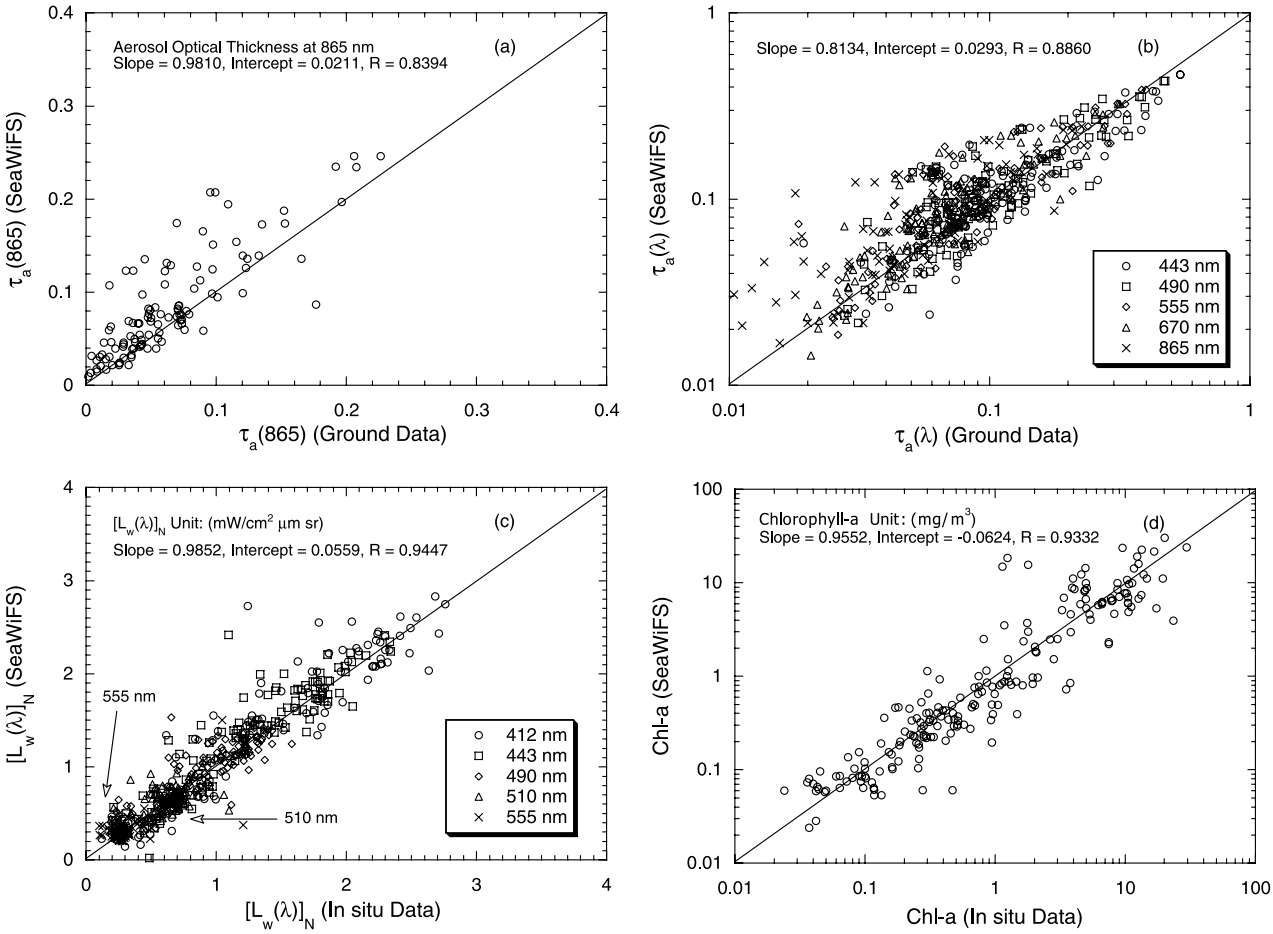

Figure 3. The SeaWiFS aerosol and ocean color products compared with the ground-based and in situ measurements for (a) $\tau_a(865)$, (b) $\tau_a(\lambda)$ at wavelengths of 443, 490, 555, 670, and 865 nm, (c) $[L_w(\lambda)]_N$ at wavelengths 412, 443, 490, 510, and 555 nm, and (d) Chl-a value. Two arrows in Figure 3c indicate two cluster data values for $[L_w(\lambda)]_N$ at 510 and 555 nm, respectively.

1 km) covering almost all oceans. The global deep water ocean region is shown in the regions in blue in Figure 2. In Figure 4, from the top to the bottom curves are for $\tau_a(865)$, $\alpha(510)$, $[L_w(443)]_N$, and Chl-a, respectively. Values of $\tau_a(865)$ and $\alpha(510)$ are indicated in the top left side, while $[L_w(443)]_N$ (mW cm^{-2} μm^{-1} sr^{-1}) and Chl-a (mg m^{-3}) values are indicated in the bottom right side (log scale). Results in Figure 4 show that the SeaWiFS $\tau_a(865)$ and $[L_w(443)]_N$ from the global deep waters have quite constant values (almost flat lines), while Chl-a has some seasonal variation and $\alpha(510)$ shows the most significant yearly repeatable variation. The coefficients of variation (standard deviation/mean) for $\tau_a(865)$, $\alpha(510)$, $[L_w(443)]_N$, and Chl-a from the global deep waters (Figure 4) are 4.5%, 21.7%, 3.7%, and 8.8%, respectively. The $\tau_a(865)$ and $\alpha(510)$ results are compared favorably with the ground-based data derived from the global open oceans for maritime aerosols [*Knobelspiesse et al.*, 2004] (see also Figure 1 for $\alpha(510)$ comparison). The SeaWiFS $\alpha(510)$ value, however, appears lower than the AERONET results which are derived from coastal and island locations [*Smirnov et al.*, 2002]. During the El Niño and La Niña in 1997–1998, Figure 4 shows abnormal aerosol and ocean color properties from the global deep ocean, in particular, for the $\alpha(510)$ value. The global deep ocean $\alpha(510)$ in 1997–1998 has similar property as in the regions of the north central Pacific and equatorial Pacific (see results of Figure 5 in the next section) where the El Niño and La Niña effects are the most significant. In general, these results indicate that SeaWiFS has very stable performance in its entire mission. However, results of

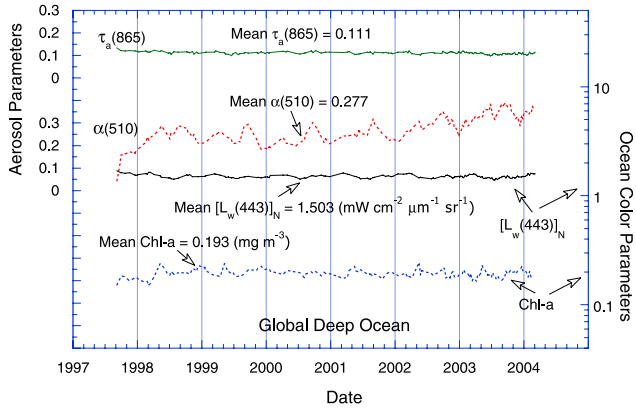

Figure 4. The mean values of the SeaWiFS aerosol ($\tau_a(865)$ and $\alpha(510)$) and ocean color ($[L_w(443)]_N$ and Chl-a) products as a function of time from the global deep waters (>1 km).

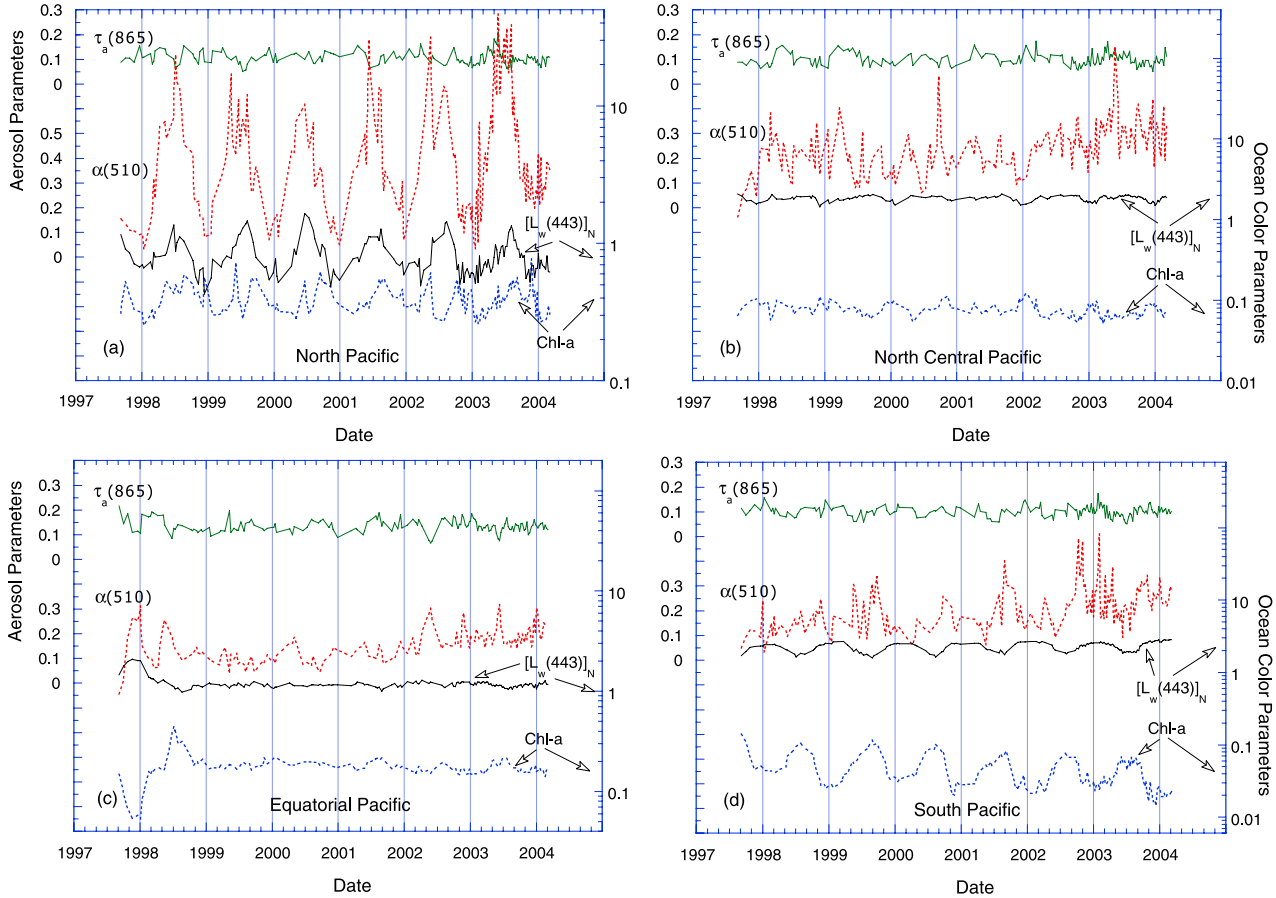

Figure 5. The mean values of the SeaWiFS aerosol ($\tau_a(865)$ and $\alpha(510)$) and ocean color ($[L_w(443)]_N$ and Chl-a) products as a function of time from the region of (a) North Pacific, (b) north central Pacific, (c) equatorial Pacific, (d) South Pacific, (e) North Atlantic, (f) South Atlantic, (g) North Indian, and (h) South Indian.

$\alpha(510)$ show a slightly up trend starting from year 2002. This is due to the SeaWiFS bands 7 and 8 change that is not exactly accounted for in the current calibration. The $\alpha(510)$ value depends on the SeaWiFS bands 7 and 8 radiance ratio and is very sensitive to the change of the relative calibration between bands 7 and 8. With the improved calibration scheme that is based on a refined lunar calibration analysis, the up trend in $\alpha(510)$ is improved. The new calibration scheme will be implemented in the SeaWiFS next data reprocessing.

4.2. Time Series From the Selected Eight Ocean Regions

[20] From the 12 major oceanographic basins defined by *Gregg et al.* [2002], we select eight regions in the global ocean as examples to study the temporal and spatial variations of the aerosol and ocean color optical properties from the SeaWiFS measurements. The selected eight ocean regions are North Pacific (NP), north central Pacific (NCP), equatorial Pacific (EP), South Pacific (SP), North Atlantic (NA), South Atlantic (SA), North Indian (NI), and South Indian (SI). The ocean regions at north central Atlantic and equatorial Atlantic are not selected because these regions have strong seasonal dust and smoke effects that SeaWiFS usually masked out for very high $\tau_a(865)$ values. Table 1 provides the name and location of the eight selected regions. The selected eight regions with $10° \times 10°$ box are also shown in Figure 2.

[21] Presented in similar way as in Figure 4, Figures 5a–5h provide the aerosol and ocean color products as a function of time. Figures 5a–5h are the SeaWiFS regional results derived from $10° \times 10°$ box for NP, NCP, EP, SP, NA, SA, NI, and SI, respectively. Comparing with results in Figure 4, the regional aerosol and ocean color products show significant seasonal and interannual variability. Each region has its own signature in the seasonal and interannual variations representing the regional geophysical and climatological influences. Overall, SeaWiFS provides stable and repeatable aerosol and ocean color results in the entire mission from September 1997 to March 2004. Table 2 provides the regional mean value with standard deviation (STD) for the aerosol and ocean color parameters derived from the SeaWiFS entire mission data. Table 3 provides the corresponding coefficient of variation (CoV) for the SeaWiFS aerosol and ocean color products. The values from the global deep waters are also presented in both Table 2 and Table 3 as references.

[22] Figure 6 provides color images for the global distributions of the SeaWiFS $\tau_a(865)$, $\alpha(510)$, $[L_w(443)]_N$, and Chl-a for the month of January and July. These images show the global spatial variations of the aerosol and ocean color properties for two different seasons. Figures 6a–6d are

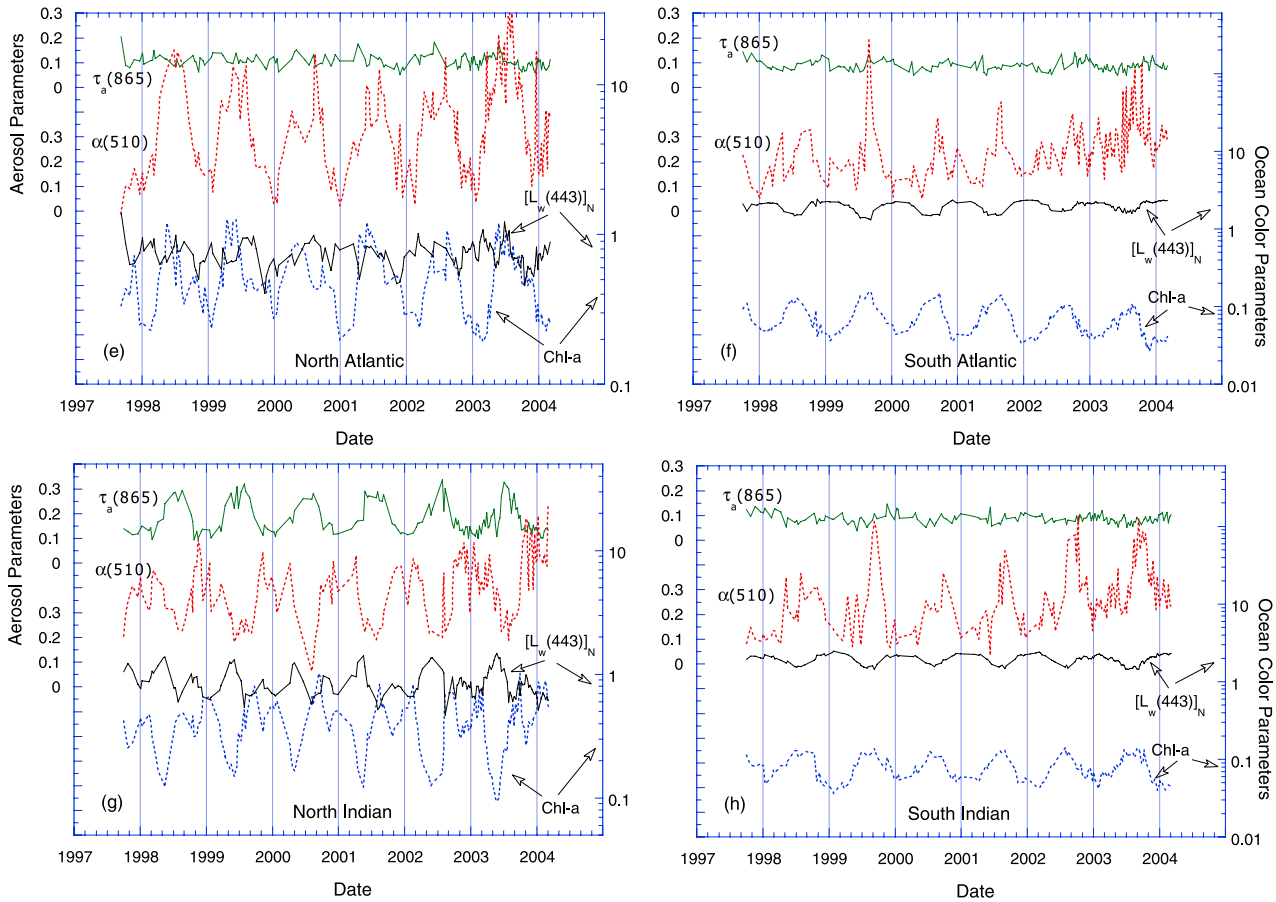

Figure 5. (continued)

$\tau_a(865)$, $\alpha(510)$, $[L_w(443)]_N$, and Chl-a global distributions for the month of January, while Figures 6e–6h are distributions for the month of July. The images were generated with measurements from the entire SeaWiFS mission (six and half years) for January and July representing monthly climatology spatial distributions. The color scales for $\tau_a(865)$, $\alpha(510)$, $[L_w(443)]_N$, and Chl-a images are indicated at the bottom of Figure 6. $\tau_a(865)$ and $\alpha(510)$ are scaled from 0 to 0.3 and −0.1 to 1.0, respectively, while $[L_w(443)]_N$ and Chl-a are scaled from 0 to 3 (mW cm^{-2} μm^{-1} sr^{-1}) and 0.01 to 10 (mg cm^{-3}), respectively. Some regional characteristics of aerosol and ocean optical properties are discussed below.

4.2.1. Pacific Ocean

[23] The NP region shows high seasonal variation of the aerosol particle size and water-leaving radiance (chlorophyll-a concentration). The results show very good interannual repeatability. The $\alpha(510)$ changes from ~0.03 in December–January to ~0.9 in June–July, while $[L_w(443)]_N$ varies from ~0.7 in December–January to ~1.4 (mW cm^{-2} μm^{-1} sr^{-1}) in June–July. The $\tau_a(865)$ value is consistently high in April (~0.13), while it is generally low in July (~0.07). The NP region has characteristics of the relative high $\alpha(510)$ value with very high variation (~60% in CoV) and very low water-leaving radiance at the blue thereby high chlorophyll-a concentration.

[24] In contrast, both the NCP and EP regions have fairly constant seasonal ocean bio-optical properties except during the El Niño and La Niña in 1997–1998 [*Chavez et al.*, 1999]. The NCP region has very clear ocean waters with mean $[L_w(443)]_N$ and Chl-a of 1.832 (mW cm^{-2} μm^{-1} sr^{-1}) and 0.076 (mg m^{-3}), respectively. However, the EP region has relative high $\tau_a(865)$ value (mean of 0.136) with relative large aerosol particle size (mean $\alpha(510)$ of 0.155). Aerosols in both the NCP and EP regions are typical of maritime aerosols. *Chou et al.* [2002] postulated that the large $\tau_a(865)$ over equatorial oceans is caused by the convergence of aerosols from subtropical regions. Strong trade winds in the tropics can produce large amount of sea salt particles [*Smirnov et al.*, 2003] and carry these aerosols to the EP region. These sea salt aerosols are characterized as large particle size (low $\alpha(510)$ value).

Table 1. Selected Eight Regions With Location of the Latitude and Longitude

Selected Regions	Location	
	Latitude	Longitude
North Pacific (NP)	50°N	150°W
North central Pacific (NCP)	25°N	150°W
Equatorial Pacific (EP)	0°	150°W
South Pacific (SP)	30°S	150°W
North Atlantic (NA)	50°N	35°W
South Atlantic (SA)	30°S	15°W
North Indian (NI)	15°N	65°E
South Indian (SI)	30°S	80°E

Table 2. Mean and Standard Deviation of the Regional Aerosol and Ocean Color Products

Selected Region	Mean Value, SD[a]			
	$\tau_a(865)$	$\alpha(510)$	$[L_w(443)]_N$ [b]	Chl-a[c]
North Pacific (NP)	0.106 ± 0.026	0.380 ± 0.226	0.820 ± 0.241	0.397 ± 0.095
North central Pacific (NCP)	0.100 ± 0.026	0.243 ± 0.102	1.832 ± 0.139	0.076 ± 0.014
Equatorial Pacific (EP)	0.136 ± 0.026	0.155 ± 0.063	1.195 ± 0.168	0.179 ± 0.045
South Pacific (SP)	0.101 ± 0.021	0.203 ± 0.087	2.289 ± 0.327	0.047 ± 0.024
North Atlantic (NA)	0.107 ± 0.025	0.332 ± 0.191	0.753 ± 0.148	0.512 ± 0.257
South Atlantic (SA)	0.089 ± 0.020	0.239 ± 0.109	1.978 ± 0.281	0.068 ± 0.031
North Indian (NI)	0.177 ± 0.062	0.393 ± 0.129	0.861 ± 0.223	0.422 ± 0.203
South Indian (SI)	0.088 ± 0.019	0.253 ± 0.123	1.956 ± 0.270	0.080 ± 0.029
Global deep water	0.111 ± 0.005	0.277 ± 0.060	1.503 ± 0.055	0.193 ± 0.017

[a]SD, standard deviation.
[b]Units of mW cm^{-2} μm^{-1} sr^{-1}.
[c]Units of mg m^{-3}.

[25] The SP region has the highest $[L_w(443)]_N$ and lowest Chl-a values in the selected ocean regions. This region is usually referred to as the ocean "desert" where macronutrient concentrations are very low [*McClain et al.*, 2004b]. The seasonal variation of $[L_w(443)]_N$ in the SP is in opposite to the NP region with high $[L_w(443)]_N$ (~2.6 (mW cm^{-2} μm^{-1} sr^{-1})) in December–January and relative low $[L_w(443)]_N$ (~1.7 (mW cm^{-2} μm^{-1} sr^{-1})) in June–July. This is because of six months seasonal shift between southern and northern oceans. Aerosols are typical of the maritime particles with mean values of $\tau_a(865) = 0.101$ and $\alpha(510) = 0.203$.

4.2.2. Atlantic Ocean

[26] The NA region has the lowest $[L_w(443)]_N$ and the highest Chl-a values with significant seasonal variations in the aerosol and ocean optical properties. The Chl-a varies from ~0.25 (mg m^{-3}) in December–January to ~1.2 (mg m^{-3}) in April–May. Both $\tau_a(865)$ and $\alpha(510)$ temporal variations in the NA region are similar to those in the NP region. However, the SA region demonstrates the similar characteristics in the atmospheric and ocean properties as for the SP region.

4.2.3. Indian Ocean

[27] The NI region has the highest $\tau_a(865)$ and $\alpha(510)$ values from the selected eight study regions with strong seasonal variations. The $\tau_a(865)$ value varies from ~0.1 in December–January to ~0.3 in June–July, while $\alpha(510)$ changes from ~0.5 in December–January to ~0.2 in June–July. The high concentration aerosols in June–July are dust contamination originated from soils in the Tigris and Euphrates basin [*Ackerman and Cox*, 1989; *Husar et al.*, 1997]. As expected, the dust has large particle size (low $\alpha(510)$ values) and large $\tau_a(865)$ value in June–July season in the NI region. There are also significant seasonal variations for the ocean color products in the NI region. Relative high Chl-a concentration and low $[L_w(443)]_N$ are also observed. It is possible that dust particles depositing to and suspension within the upper layer of the ocean may have some effects on the results of the low $[L_w(443)]_N$ value in the region [*Claustre et al.*, 2002]. On contrast, the SI region shows constantly clear atmosphere (lowest $\tau_a(865)$) and oceans (low Chl-a and high $[L_w(443)]_N$). The atmospheric and ocean properties in the SI region are similar to those in the SP and SA regions.

4.3. Seasonal Variations and Correlation Analyses

[28] To better understand temporal and spatial variation of the SeaWiFS aerosol and ocean color products, we computed the monthly mean values for $\tau_a(865)$, $\alpha(510)$, $[L_w(443)]_N$, and Chl-a and analyzed correlation among these parameters. Figure 7 provides mean values for $\tau_a(865)$, $\alpha(510)$, $[L_w(443)]_N$, and Chl-a, which were derived from the SeaWiFS entire mission data, as a function of the month for the selected eight ocean regions. Figure 7 is presented similarly as in Figure 5 except x axis is in month instead of year. Thus the seasonal variations in aerosol and ocean color parameters can be clearly seen. In addition, the correlation coefficients between various aerosol and ocean color parameters for the eight ocean regions were computed and provided in Table 4. In Table 4, correlation coefficients are provided for the SeaWiFS parameters of $\tau_a(865)$ and $\alpha(510)$, $\tau_a(865)$ and $[L_w(443)]_N$, $\tau_a(865)$ and Chl-a, $\alpha(510)$ and $[L_w(443)]_N$, and $\alpha(510)$ and Chl-a. The correlation coefficient for $[L_w(443)]_N$ and Chl-a is not computed because these two is usually strongly correlated, i.e., low Chl-a generally corresponding to high $[L_w(443)]_N$ and vice versa (see Figure 6) [*Gordon et al.*, 1988; *Morel*, 1988; *O'Reilly et al.*, 1998]. By carefully examining the correlation coefficients in Table 4 and results in Figures 5 and 7, we have not found any obvious artifacts that were introduced from the SeaWiFS atmospheric correction and aerosol retrieval algorithms. Specifically, there is no obvious systematic correlation between aerosol and ocean color products, e.g., mistakenly accounting for the ocean contribution as from aerosol radiance.

4.4. Some Regional Data Analyses and Discussions

[29] Both the NP and NA regions show significant elevation of the $\alpha(510)$ values during June–July season (see results in Figures 6f, 7a, and 7e), while the $\tau_a(865)$

Table 3. Coefficient of Variation for the SeaWiFS Regional Aerosol and Ocean Color Products

Selected Region	Coefficient of Variation, %			
	$\tau_a(865)$	$\alpha(510)$	$[L_w(443)]_N$	Chl-a
North Pacific (NP)	24.5	59.5	29.4	23.9
North central Pacific (NCP)	26.0	42.0	7.6	18.4
Equatorial Pacific (EP)	19.1	40.6	14.1	25.1
South Pacific (SP)	20.8	42.9	14.3	51.1
North Atlantic (NA)	23.4	57.5	19.7	50.2
South Atlantic (SA)	22.5	45.6	14.2	45.6
North Indian (NI)	35.0	32.8	25.9	48.1
South Indian (SI)	21.6	48.6	13.8	36.3
Global deep water	4.5	21.7	3.7	8.8

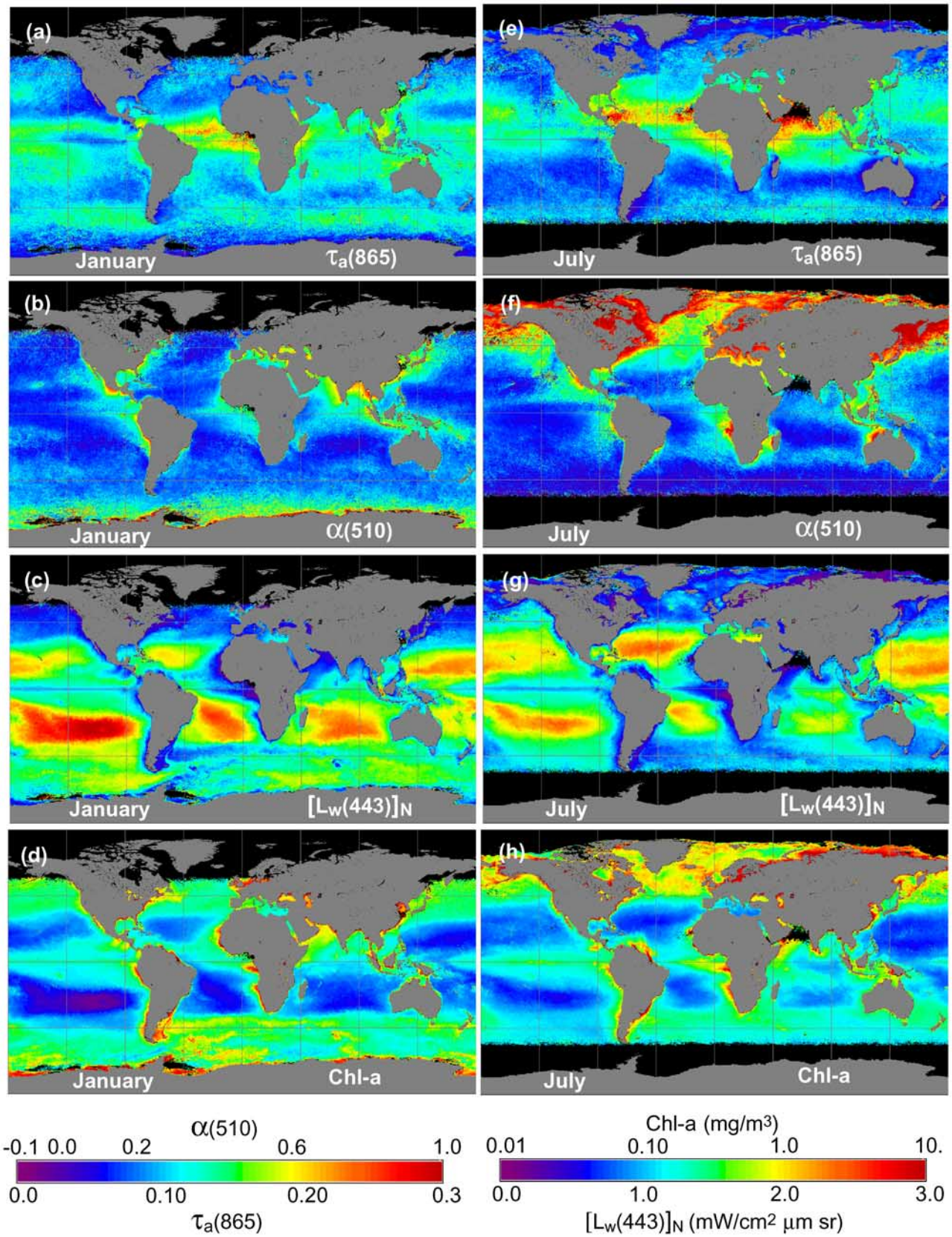

Figure 6. The color images for the global distributions of the SeaWiFS $\tau_a(865)$, $\alpha(510)$, $[L_w(443)]_N$, and Chl-a for the month of (a–d) January and (e–h) July.

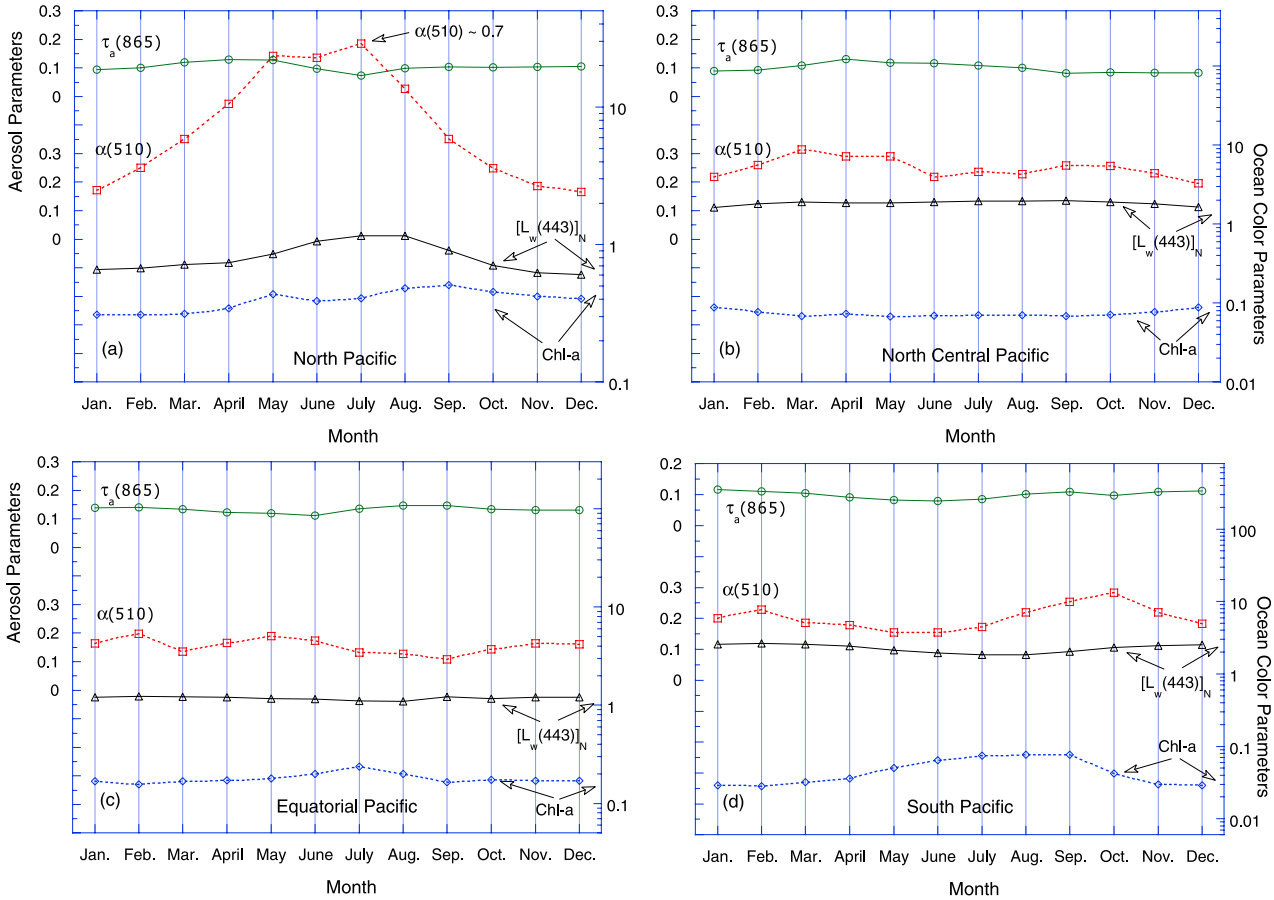

Figure 7. The SeaWiFS monthly mean values of $\tau_a(865)$, $\alpha(510)$, $[L_w(443)]_N$, and Chl-a derived from the entire SeaWiFS mission data for region of (a) North Pacific, (b) north central Pacific, (c) equatorial Pacific, (d) South Pacific, (e) North Atlantic, (f) South Atlantic, (g) North Indian, and (h) South Indian.

values are relatively flat. For the NP region, the highest mean $\tau_a(865)$ value (~0.13) appears in the month of April, while in July the mean $\tau_a(865)$ value is the lowest (~0.07) with the highest of the mean $\alpha(510)$ value (~0.7). The high AOT in April in the Northern Hemisphere was also reported by other investigators [*Husar et al.*, 1997; *Mishchenko et al.*, 1999]. The seasonal variation of $\alpha(510)$ in the NP and NA regions is consistent with the seasonal change of the ocean DMS emission in these regions [*Kettle et al.*, 1999], as well as the global anthropogenic sulfate production efficiency variation (low in January and high in July) [*Chin et al.*, 2000]. *Kettle et al.* [1999] observed significant elevation of the DMS emission in the NP and NA regions from January to July, and concluded that there was no significant correlation between the global DMS distributions and ocean physical (temperature and salinity) and biological (chlorophyll concentration) parameters. However, *Andreae et al.* [1994] found some correlation between DMS emission and Chl-a in the tropical South Atlantic. In the NP region, SeaWiFS measurements show some positive correlation between $\alpha(510)$ and $[L_w(443)]_N$ (R = 0.613), while there is evidence of positive correlation between $\alpha(510)$ and Chl-a (R = 0.581) in the NA region. It is interesting to note that, with increase of the DMS emission in June–July season in the NP and NA regions, one might expect increase of $\tau_a(865)$. This is not shown in the SeaWiFS results due probably to effects of particle extinction coefficient, i.e., $\tau_a(865)$ depends both on the particle concentration and its extinction coefficient (scattering and absorption efficiency). Results from *Chin et al.* [2002] using a chemical model coupled to the atmospheric circulation that has incorporated the natural and anthropogenic sulfate cycle contributions [*Chin et al.*, 2000] also do not show the increase of the AOT in July in the NP region. However, these discussions are preliminary. Further investigations with the in situ particle size and its concentration measurements are needed.

[30] The NI region shows large negative correlation (−0.726) between $\tau_a(865)$ and $\alpha(510)$, representing the seasonal dust contamination in the NI region. However, significantly low $\alpha(510)$ values with slightly negative correlation (−0.319) between $\tau_a(865)$ and $\alpha(510)$ are observed at the EP region. This could be result of sea salt particles that are produced in tropics and carried out to the EP region with strong trade winds [*Chou et al.*, 2002]. Study shows that properties of large sea salt aerosols at the tropics are strongly correlated to the wind speed with negative correlation between the AOT and Ångström exponent [*Smirnov et al.*, 2003].

5. Conclusions

[31] Since September of 1997, SeaWiFS has routinely produced the aerosol and ocean color products over the

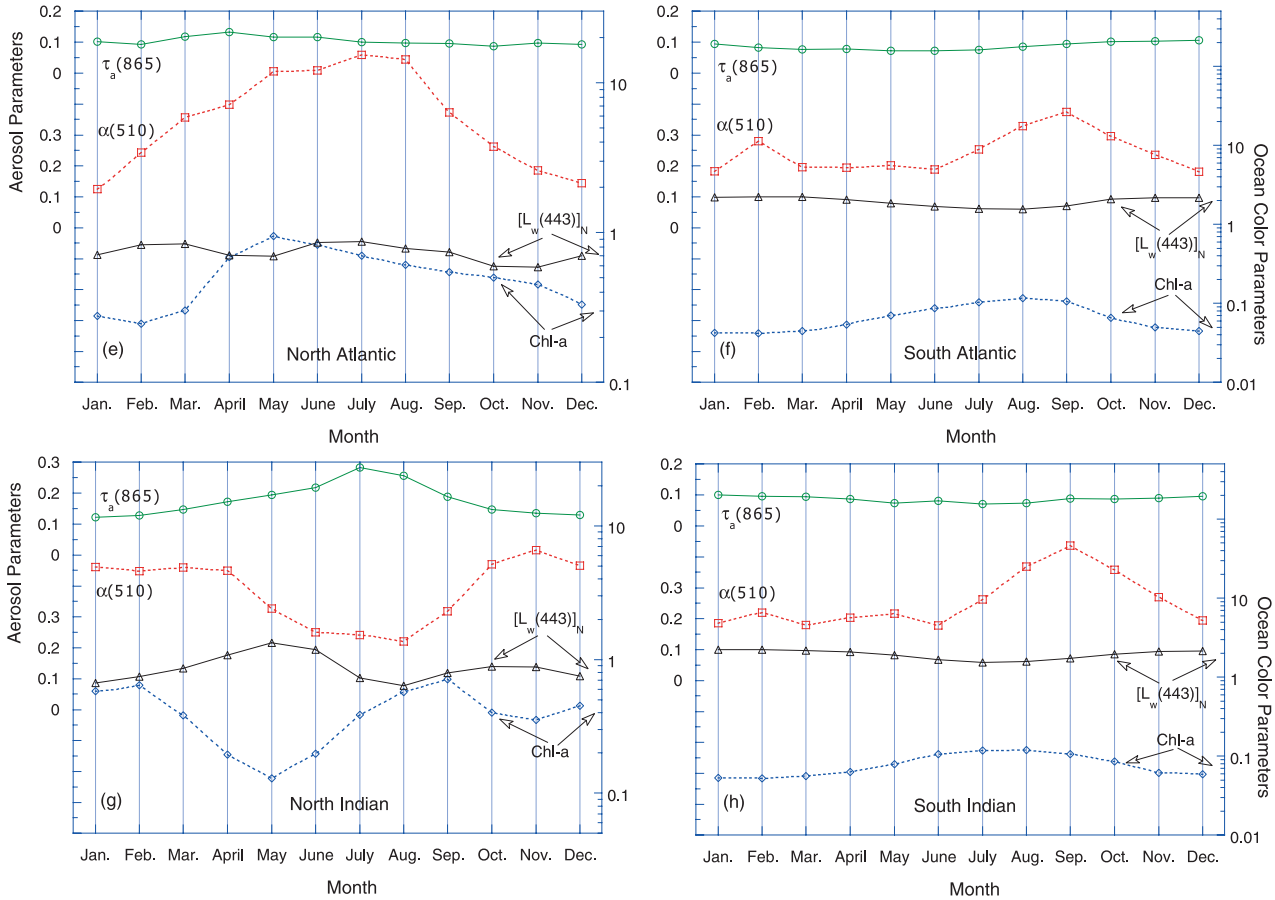

Figure 7. (continued)

global ocean. The SeaWiFS aerosol retrieval algorithm uses the aerosol spectral radiances measured at the SeaWiFS 765 and 865 nm bands to derive appropriate aerosol models and aerosol optical properties, e.g., the AOT at 865 nm and the Ångström exponent from 510 and 865 nm. The SeaWiFS algorithm uses 12 aerosol models that are nonabsorbing and weakly absorbing for generating the aerosol lookup tables. In comparing with the ground-based data collected from the global oceans through the SIMBIOS project, the Ångström exponents from the SeaWiFS 12 aerosol models represent well for aerosols in the maritime environment. There are continuous efforts within the ocean community to collect the ground-based aerosol and in situ ocean color data to calibrate, validate, and improve the satellite-retrieved aerosol and ocean color products.

[32] To improve data quality, the SeaWiFS entire aerosol and ocean color products have been reprocessed completely four times since September 1997. The SeaWiFS aerosol and ocean color products compare generally well with the ground-based and in situ measurements. However, in comparing with the ground-based data, the SeaWiFS-derived AOT at 865 nm may have slightly over-estimated (~5–10%), while there is under-estimation for the Ångström exponent (difference varies significantly depending on values). Both SeaWiFS aerosol and ocean color products show very stable and repeatable results in the entire mission, implying that SeaWiFS is well characterized and calibrated. After more than six and half years of operation, SeaWiFS still has very good sensor performance. By carefully examining the SeaWiFS aerosol and ocean color results, we have

Table 4. Correlation Coefficients of Aerosol and Ocean Color Parameters for the Eight Ocean Regions

	Correlation Coefficient				
Selected Region	$\tau_a(865)$ and $\alpha(510)$	$\tau_a(865)$ and $[L_w(443)]_N$	$\tau_a(865)$ and Chl-a	$\alpha(510)$ and $[L_w(443)]_N$	$\alpha(510)$ and Chl-a
North Pacific (NP)	−0.026	−0.185	0.023	0.613	0.155
North central Pacific (NCP)	−0.116	0.097	0.256	0.126	−0.406
Equatorial Pacific (EP)	−0.319	0.099	−0.111	0.166	−0.247
South Pacific (SP)	−0.147	0.311	−0.129	0.149	−0.211
North Atlantic (NA)	−0.045	0.319	0.118	0.203	0.581
South Atlantic (SA)	−0.146	0.230	0.037	−0.254	0.226
North Indian (NI)	−0.726	0.036	−0.131	−0.114	0.062
South Indian (SI)	−0.423	0.411	−0.198	−0.423	0.356

not found any correlation artifacts between aerosol and ocean color products that are resulted from the performance of the SeaWiFS atmospheric correction and aerosol retrieval algorithms.

[33] The atmosphere and ocean interactively influence the regional geophysical and climatological variations, e.g., emission of the DMS from ocean surface modifies aerosol optical and radiative properties, while dust depositing to and suspension within the upper layer of the ocean changes the ocean properties. Therefore it is important and useful to study the global aerosol and ocean spatial and temporal variation collectively with the simultaneous aerosol and ocean color measurements. As examples, we presented some detailed analyses for the eight regions selected from the global ocean with the simultaneous SeaWiFS aerosol and ocean color data. These results provide good examples of the regional significance in the seasonal and interannual variations that are influenced by the regional geophysical and climatological changes.

[34] **Acknowledgments.** The authors are grateful to the SeaBASS investigators who have contributed valuable data through the SeaWiFS and SIMBIOS calibration and validation programs. We thank S. Bailey for providing help in the matchup analyses and two anonymous reviewers for their helpful comments. This research was supported by the NASA SIMBIOS grant NAS5-00203 and the NASA NPP grant NNG04GE05A (MW). The SeaWiFS ocean color mission is a joint venture of NASA and ORBIMAGE.

References

Ackerman, S. A., and S. K. Cox (1989), Surface weather observations of atmospheric dust over the southeast summer monsoon region, *Meteorol. Atmos. Phys.*, *41*, 19–349.

Andreae, T. W., M. O. Andreae, and G. Schebeske (1994), Biogenic sulfur emissions and aerosol over the tropical South Atlantic: 1. Dimethylsulfide in seawater and in the atmospheric boundary layer, *J. Geophys. Res.*, *99*, 22,819–22,829.

Antoine, D., and A. Morel (1999), A multiple scattering algorithm for atmospheric correction of remotely sensed ocean colour (MERIS instrument): Principle and implementation for atmospheres carrying various aerosols including absorbing ones, *Int. J. Remote Sens.*, *20*, 1875–1916.

Charlson, R. J., J. E. Lovelock, M. O. Andreae, and S. G. Warren (1987), Oceanic phytoplankton, atmospheric sulphur, cloud albedo and climate, *Nature*, *326*, 655–661.

Charlson, R. J., S. E. Schwartz, J. M. Hales, R. D. Cess, J. A. Coakley, J. E. Hansen, and D. J. Hofmann (1992), Climate forcing by anthropogenic aerosols, *Science*, *255*, 423–430.

Chavez, F. P., P. G. Strutton, G. E. Friederich, R. A. Feely, G. C. Feldman, D. G. Foley, and M. J. McPhaden (1999), Biological and chemical response of the equatorial Pacific Ocean to the 1997–98 El Niño, *Science*, *286*, 2126–2131.

Chin, M., R. B. Rood, S. J. Lin, J. F. Müller, and A. M. Thompson (2000), Atmospheric sulfur cycle simulated in the global model GOCART: Model description and global properties, *J. Geophys. Res.*, *105*, 24,671–24,687.

Chin, M., P. Ginoux, S. Kinne, O. Torres, B. N. Holben, B. N. Duncan, R. V. Martin, J. A. Logan, A. Higurashi, and T. Nakajima (2002), Tropospheric aerosol optical thickness from the GOCART model and comparisons with satellite and Sun photometer measurements, *J. Atmos. Sci.*, *59*, 461–483.

Chou, M. D., P. K. Chan, and M. Wang (2002), Aerosol radiative forcing derived from SeaWiFS-retrieved aerosol optical properties, *J. Atmos. Sci.*, *59*, 748–757.

Claustre, H., A. Morel, S. B. Hooker, M. Babin, D. Antoine, K. Oubelkheir, A. Bricaud, K. Leblanc, B. Quéguiner, and S. Maritorena (2002), Is desert dust making oligotrophic waters greener?, *Geophys. Res. Lett.*, *29*(10), 1469, doi:10.1029/2001GL014056.

d'Almeida, G. A., P. Koepke, and E. P. Shettle (1991), *Atmospheric Aerosols: Global Climatology and Radiative Characteristics*, 561 pp., A. Deepak, Hampton, Va.

Deschamps, P.-Y., B. Fougnie, R. Frouin, P. Lecomte, and C. Verwaerde (2004), SIMBAD: A field radiometer for satellite ocean-color validation, *Appl. Opt.*, *43*, 4055–4069.

Deuze, J. L., et al. (2001), Remote sensing of aerosols over land surfaces from POLDER-ADEOS-1 polarized measurements, *J. Geophys. Res.*, *106*, 4913–4926.

Fargion, G. S., and C. R. McClain (2003), An overview of SIMBIOS program activities and accomplishments, in *SIMBIOS Project 2003 Annual Report*, *NASA Tech. Memo. 2003–212251*, pp. 1–33, NASA Goddard Space Flight Cent., Greenbelt, Md.

Frouin, R., M. Schwindling, and P. Y. Deschamps (1996), Spectral reflectance of sea foam in the visible and near infrared: In situ measurements and remote sensing implications, *J. Geophys. Res.*, *101*, 14,361–14,371.

Fukushima, H., A. Higurashi, Y. Mitomi, T. Nakajima, T. Noguchi, T. Tanaka, and M. Toratani (1998), Correction of atmospheric effects on ADEOS/OCTS ocean color data: Algorithm description and evaluation of its performance, *J. Oceanogr.*, *54*, 417–430.

Gordon, H. R. (1997), Atmospheric correction of ocean color imagery in the Earth Observing System era, *J. Geophys. Res.*, *102*, 17,081–17,106.

Gordon, H. R., and M. Wang (1992), Surface roughness considerations for atmospheric correction of ocean color sensors. 1: The Rayleigh scattering component, *Appl. Opt.*, *31*, 4247–4260.

Gordon, H. R., and M. Wang (1994a), Retrieval of water-leaving radiance and aerosol optical thickness over the oceans with SeaWiFS: A preliminary algorithm, *Appl. Opt.*, *33*, 443–452.

Gordon, H. R., and M. Wang (1994b), Influence of oceanic whitecaps on atmospheric correction of ocean-color sensor, *Appl. Opt.*, *33*, 7754–7763.

Gordon, H. R., D. K. Clark, J. L. Mueller, and W. A. Hovis (1980), Phytoplankton pigments from the Nimbus-7 coastal zone color scanner: Comparisons with surface measurements, *Science*, *210*, 63–66.

Gordon, H. R., O. B. Brown, R. H. Evans, J. W. Brown, R. C. Smith, K. S. Baker, and D. K. Clark (1988), A semianalytic radiance model of ocean color, *J. Geophys. Res.*, *93*, 10,909–10,924.

Gregg, W. W., M. E. Conkright, J. E. O'Reilly, F. S. Patt, M. Wang, J. Yoder, and N. Casey-McCabe (2002), NOAA-NASS coastal zone color scanner reanalysis effort, *Appl. Opt.*, *41*, 1615–1628.

Hale, G. M., and M. R. Querry (1973), Optical constants of water in the 200nm to 200(m wavelength region, *Appl. Opt.*, *12*, 555–563.

Holben, B. N., et al. (1998), AERONET—A federated instrument network and data archive for aerosol characterization, *Remote Sens. Environ.*, *66*, 1–16.

Hooker, S. B., W. E. Esaias, G. C. Feldman, W. W. Gregg, and C. R. McClain (1992), *An Overview of SeaWiFS and Ocean Color*, *SeaWiFS Tech. Rep. Ser.*, vol. 1, *NASA Tech. Memo. 104566*, edited by S. B. Hooker and E. R. Firestone, NASA Goddard Space Flight Cent., Greenbelt, Md.

Husar, R. B., J. M. Prospero, and L. L. Stowe (1997), Characterization of tropospheric aerosols over the oceans with the NOAA advanced very high resolution radiometer optical thickness operational product, *J. Geophys. Res.*, *102*, 16,889–16,909.

Husar, R. B., et al. (2001), Asian dust events of April 1998, *J. Geophys. Res.*, *106*, 18,317–18,330.

Ignatov, A., and L. Stowe (2002), Aerosol retrievals from individual AVHRR channels: I. Retrieval algorithm and transition from Dave to 6S radiative transfer model, *J. Atmos. Sci.*, *59*, 313–334.

Kaufman, Y. J., D. Tanré, L. Remer, E. Vermote, and B. N. Holben (1997), Operational remote sensing of tropospheric aerosols over the land from EOS-MODIS, *J. Geophys. Res.*, *102*, 17,051–17,068.

Kaufman, Y. J., D. Tanré, and O. Boucher (2002), A satellite view of aerosols in the climate system, *Nature*, *419*, 215–223.

Kettle, A. J., et al. (1999), A global database of sea surface dimethylsulfide (DMS) measurements and a procedure to predict sea surface DMS as a function of latitude, longitude, and month, *Global Biogeochem. Cycles*, *13*, 399–444.

Kiehl, J. T., and B. P. Briegleb (1993), The relative roles of sulfate aerosols and greenhouse gases in climate forcing, *Science*, *260*, 311–314.

King, M. D., Y. J. Kaufman, D. Tanré, and T. Nakajima (1999), Remote sensing of tropospheric aerosols from space: Past, present, and future, *Bull. Am. Meteorol. Soc.*, *80*, 2229–2259.

Knobelspiesse, K. D., C. Pietras, G. S. Fargion, M. Wang, R. Frouin, M. A. Miller, A. Subramaniam, and W. M. Balch (2004), Maritime aerosol optical properties measured by handheld Sun photometers, *Remote Sens. Environ.*, *93*, 26–106.

Maritorena, S., D. A. Siegel, and A. Peterson (2002), Optimization of a semi-analytical ocean color model for global scale applications, *Appl. Opt.*, *41*, 2705–2714.

Martonchik, J. V., D. J. Diner, R. A. Kahn, T. P. Ackerman, M. E. Verstraete, B. Pinty, and H. R. Gordon (1998), Techniques for the retrieval of aerosol properties over land and ocean using multiangle imaging, *IEEE Trans. Geosci. Remote Sens.*, *36*, 1212–1227.

McClain, C., W. Esaias, G. Feldman, R. Frouin, W. Gregg, and S. Hooker (2002), The proposal for the NASA Sensor Intercalibration and Merger

for Biological and Interdisciplinary Oceanic Studies (SIMBIOS) Program, 1995, *NASA Tech. Memo. 2002-210008,* 54 pp., NASA Goddard Space Flight Cent., Greenbelt, Md.

McClain, C. R., G. C. Feldman, and S. B. Hooker (2004a), An overview of the SeaWiFS project and strategies for producing a climate research quality global ocean bio-optical time series, *Deep Sea Res. Part II*, *51*, 5–42.

McClain, C. R., S. R. Signorini, and J. R. Christian (2004b), Subtropical gyre variability observed by ocean-color satellites, *Deep Sea Res. Part II*, *51*, 281–301.

Mishchenko, M. I., I. V. Geogdzhayev, B. Cairns, W. B. Rossow, and A. A. Lacis (1999), Aerosol retrievals over the ocean by use of channels 1 and 2 AVHRR data: Sensitivity analysis and preliminary results, *Appl. Opt.*, *38*, 7325–7341.

Moore, K. D., K. J. Voss, and H. R. Gordon (2000), Spectral reflectance of whitecaps: Their contribution to water-leaving radiance, *J. Geophys. Res.*, *105*, 6493–6499.

Morel, A. (1988), Optical modeling of the upper ocean in relation to its biogenous matter content (case 1 waters), *J. Geophys. Res.*, *93*, 10,749–10,768.

Morys, M., F. M. Mims, S. Hagerup, S. E. Anderson, A. Baker, J. Kia, and T. Walkup (2001), Design, calibration, and performance of MICROTOPS II handheld ozone monitor and Sun photometer, *J. Geophys. Res.*, *106*, 14,573–14,582.

Moulin, C., H. R. Gordon, V. F. Banzon, and R. H. Evans (2001a), Assessment of Saharan dust absorption in the visible from SeaWiFS imagery, *J. Geophys. Res.*, *106*, 18,239–18,249.

Moulin, C., H. R. Gordon, R. M. Chomko, V. F. Banzon, and R. H. Evans (2001b), Atmospheric correction of ocean color imagery through thick layers of Saharan dust, *Geophys. Res. Lett.*, *28*, 5–8.

Mueller, J. M., and G. S. Fargion (2002), Ocean optics protocols for satellite ocean color sensor validation, Revision 3, Part I and II, *NASA Tech. Memo. 2002-210004*, 308 pp., NASA Goddard Space Flight Cent., Greenbelt, Md.

Myhre, G., et al. (2005), Intercomparison of satellite retrieved aerosol optical depth over ocean during the period September 1997 to December 2000, *Atmos. Chem. Phys.*, in press.

Nakajima, T., and A. Higurashi (1998), A use of two-channel radiances for an aerosol characterization from space, *Geophys. Res. Lett.*, *25*, 3815–3818.

O'Reilly, J. E., S. Maritorena, B. G. Mitchell, D. A. Siegel, K. L. Carder, S. A. Garver, M. Kahru, and C. R. McClain (1998), Ocean color chlorophyll algorithms for SeaWiFS, *J. Geophys. Res.*, *103*, 24,937–24,953.

Patt, F. S., et al. (2003), *Algorithm Updates for the Fourth SeaWiFS Data Reprocessing*, *SeaWiFS Postlaunch Tech. Rep. Ser.*, vol. 22, *NASA Tech. Memo. 2003-206892*, edited by S. B. Hooker and E. R. Firestone, 74 pp., NASA Goddard Space Flight Cent., Greenbelt, Md.

Rao, C. R. N., L. L. Stowe, and E. P. McClain (1989), Remote sensing of aerosols over the oceans using AVHRR data: Theory, practice, and applications, *Int. J. Remote Sens.*, *10*, 743–749.

Reynolds, M. R., M. A. Miller, and M. J. Bartholomew (2002), A fast-rotating spectral shadowband radiometer for marine applications, *J. Atmos. Ocean. Tech.*, *18*, 200–214.

Shettle, E. P., and R. W. Fenn (1979), Models for the aerosols of the lower atmosphere and the effects of humidity variations on their optical properties, *Rep. AFGL-TR-79-0214*, U.S. Air Force Geophys. Lab., Hanscom AFB, Mass.

Siegel, D. A., M. Wang, S. Maritorena, and W. Robinson (2000), Atmospheric correction of satellite ocean color imagery: The black pixel assumption, *Appl. Opt.*, *39*, 3582–3591.

Smirnov, A., B. N. Holben, Y. J. Kaufman, O. Dubovik, T. F. Eck, I. Slutsker, C. Pietras, and R. N. Halthore (2002), Optical properties of atmospheric aerosol in maritime environments, *J. Atmos. Sci.*, *59*, 501–523.

Smirnov, A., B. N. Holben, T. F. Eck, O. Dubovik, and I. Slutsker (2003), Effect of wind speed on columnar aerosol optical properties at Midway Island, *J. Geophys. Res.*, *108*(D24), 4802, doi:10.1029/2003JD003879.

Smith, R. C., and K. S. Baker (1981), Optical properties of the clearest natural waters, *Appl. Opt.*, *20*, 177–184.

Stumpf, R. P., R. A. Arnone, R. W. Gould, P. M. Martinolich, and V. Ransibrahmanakul (2003), *A Partially Coupled Ocean-Atmosphere Model for Retrieval of Water-Leaving Radiance From SeaWiFS in Coastal Waters*, *SeaWiFS Postlaunch Tech. Rep. Ser.*, vol. 22, *NASA Tech. Memo. 2003-206892*, edited by S. B. Hooker and E. R. Firestone, pp. 51–59, NASA Goddard Space Flight Cent., Greenbelt, Md.

Tanré, D., Y. J. Kaufman, M. Herman, and S. Mattoo (1997), Remote sensing of aerosol properties over oceans using the MODIS/EOS spectral radiances, *J. Geophys. Res.*, *102*, 16,971–16,988.

Tanré, D., F. M. Bréon, J. L. Deuzé, M. Herman, P. Goloub, F. Nadal, and A. Marchand (2001), Global observation of anthropogenic aerosols from satellite, *Geophys. Res. Lett.*, *28*, 4555–4558.

Torres, O., J. R. Herman, Z. Ahmad, and J. Gleason (1998), Derivation of aerosol properties from satellite measurements of backscattered ultraviolet radiation: Theoretical basis, *J. Geophys. Res.*, *103*, 17,099–17,110.

Wang, M. (2000), *The SeaWiFS Atmospheric Correction Algorithm Updates*, *SeaWiFS Postlaunch Tech. Rep. Ser.*, vol. 9, *NASA Tech. Memo. 2000-206892*, edited by S. B. Hooker and E. R. Firestone, pp. 57–63, NASA Goddard Space Flight Cent., Greenbelt, Md.

Wang, M. (2002), The Rayleigh lookup tables for the SeaWiFS data processing: Accounting for the effects of ocean surface roughness, *Int. J. Remote Sens.*, *23*, 2693–2702.

Wang, M., and S. Bailey (2001), Correction of the Sun glint contamination on the SeaWiFS ocean and atmosphere products, *Appl. Opt.*, *40*, 4790–4798.

Wang, M., and B. A. Franz (2000), Comparing the ocean color measurements between MOS and SeaWiFS: A vicarious intercalibration approach for MOS, *IEEE Trans. Geosci. Remote Sens.*, *38*, 184–197.

Wang, M., and H. R. Gordon (1994), Estimating aerosol optical properties over the oceans with the Multiangle Imaging Spectroradiometer: Some preliminary studies, *Appl. Opt.*, *33*, 4042–4057.

Wang, M., A. Isaacman, B. A. Franz, and C. R. McClain (2002), Ocean color optical property data derived from the Japanese ocean color and temperature scanner and the French polarization and directionality of the Earth's reflectances: A comparison study, *Appl. Opt.*, *41*, 974–990.

Werdell, P. J., S. Bailey, G. Fargion, C. Pietras, K. Knobelspiesse, G. Feldman, and C. R. McClain (2003), Unique data repository facilitates ocean color satellite validation, *Eos Trans. AGU*, *84*(38), 377.

Yang, H., and H. R. Gordon (1997), Remote sensing of ocean color: Assessment of water-leaving radiance bidirectional effects on atmospheric diffuse transmittance, *Appl. Opt.*, *36*, 7887–7897.

K. D. Knobelspiesse, NASA Goddard Institute for Space Studies, 2880 Broadway, New York, NY 10025, USA.

C. R. McClain, Code 970.2, NASA Goddard Space Flight Center, Greenbelt, MD 20771, USA.

M. Wang, NOAA/NESDIS/ORA, E/RA3, Room 102, 5200 Auth Road, Camp Springs, MD 20746, USA. (menghua.wang@noaa.gov)